Bull. Chem. Soc. Ethiop. **2023**, 37(2), 391-404.
DOI: https://dx.doi.org/10.4314/bcse.v37i2.11

ISSN 1011-3924
Printed in Ethiopia
Online ISSN 1726-801X

ZEOLITE A/$ZnCl_2$ NANOPARTICLES AS A CATALYST FOR ECO-FRIENDLY SYNTHESIS OF PYRAZOLE-1-CARBOTHIOAMIDES WITH DOCKING VALIDATION AS COVID-19 MAIN PROTEASE (MPRO) INHIBITOR

Norhan M. Younis[1], Amr M. Abdelghany[2], Fathy Shaaban[3,4], Tamer K. Khatab[5], Ehab Abdel-Latif[1] and Heba M. Metwally[1*]

[1]Chemistry Department, Faculty of Science, Mansoura University, 35516 Mansoura, Egypt
[2]Spectroscopy Department, Physics Research Institute, National Research Centre, 33 ElBehouth St., Dokki, 12311 Giza, Egypt
[3]Environment and Health Research Department, The Custodian of the Two Holy Mosques Institute for Hajj and Umrah Research, Umm Al-Qura University, 21421 Makkah, Saudi Arabia
[4]Geomagnetic and Geoelectric Department, National Research Institute of Astronomy and Geophysics, Egypt
[5]Organometallic and Organometalloid Chemistry Department, National Research Centre, 33 ElBehouth St., Dokki, 12622 Giza, Egypt

(Received September 13, 2022; Revised October 1, 2022; Accepted October 17, 2022)

ABSTRACT. The synthesized Zeolite A/$ZnCl_2$ nanoparticles via the hydrothermal route were characterized using FTIR, XRD, and SEM/EDAX techniques. The characterized catalyst was used for the eco-friendly synthesis of 4,5-dihydro-pyrazole-1-carbothioamide derivatives. Under solvent-free conditions, a multi-component reaction between hydrazine, isothiocyanate, and chalcone was done with a prepared nano-catalyst as an inexpensive, recyclable, easy-to-get, and nontoxic catalyst. The molecular docking study explained that dihydro-1-carbothioamide pyrazoles can be considered COVID-19 main protease (M^{pro}) inhibitors. In order to investigate the 3D conformation of the compounds that were synthesized, the density functional theory (DFT) was applied with a B3LYP hybrid functional and a 6-311++ G(d,p) basis set. This allowed us to investigate the compounds' electronic and charge transfer properties. In this series of compounds, the derivative 30d showed the lowest HOMO–LUMO energy gap.

KEY WORDS: Zeolite A/$ZnCl_2$ nanoparticles, Pyrazole-1-carbothioamides, Docking, XRD, SEM/EDX, HRTEM

INTRODUCTION

Azoles are presented as important scaffolds with a five-membered ring in many natural and biological heterocyclic compounds. Natural organic compounds based on pyrazole are difficultly synthesized by living organisms and the formation of N-N bond is not an easy process in biosynthesis [1]. The pyrazole ring has been reported in 1966, then being essentially used as a part of pharmacophore in hypnotic drugs. The first cytotoxic pyrazole, phenylahistin, were isolated from natural sources in 1969 separated from the marine sponge *Leucetta microraphis* found on Australia's Great Barrier Reef, exhibited important biological activities, such as anti-cancer or neurotoxic effects [2, 3]. Pyrazole ring contains the two main types of nitrogen, pyrrole like N which gives the acidic character, and aromaticity in addition to pyridine like N which gives the basic character. From this, the pyrazole ring has considered an electron-rich ring and has versatile chemical properties, and is employed in a lot of organic syntheses. Pyrazole ring exhibited two types of reactions; electrophilic and nucleophilic [4-7]. The nucleophilic nature was displayed from three positions (N1, N2, C4), in addition two electrophilic nature was displayed from two positions (C3, C5). Knowing that, depending on the reaction conditions, electrophilic addition takes place most often at C4 and/or to one of the two nitrogen atoms. Substitution at an

*Corresponding author. E-mail: hebama@mans.edu.eg

annular carbon can only be accomplished via coupling reactions such as Suzuki couplings [8]. For boronic acid or ester cross-coupling to happen at the intended position, halogens must be present in C4 [9]. Pyrazole derivatives showed abroad spectrum of biological effects, for instance, anti-tubercular, antifungal, antimalarial, anticancer, and anti-AIDS [10-16]. Pyrazole and its derivatives are also considered as possible antimicrobial, antiepileptic, anti-inflammatory, antipsychotic, antidepressant, inhibitors of protein kinases, anti-aggregating, antiarthritic, cerebro protectors, reverse transcriptase inhibitor, a COX-2 inhibitor, nematocidal and soluble guanylate cyclase activity, etc [17]. Pyrazole and its derivatives have been found to be bioactive parts of commercially available therapies like deramaxx (NSAID), pyrazomycin and difenamizole (anticancer drugs), and floxan and difenamizole (anti-inflammatory drugs) (Figure 1). Zeolites are famous aluminosilicate material which is commercial used as adsorbent, catalyst in organic synthesis [18] and petrochemical processes [19]. Zeolites are potentially attractive heterogeneous catalyst due to the easy recovery of product/substrate, catalyst recycling, and possible regioselectivity, easy to separate, environmentally friendly [20-23]. Zn-loaded zeolites showing increasing surface acidity [24] and are suitable catalyst for heterocyclization [25]. Zeolite nano-particles showed improved catalytic performance because of the increase in mass diffusion; and could enhance the catalytic activity as a result of the increased accessibility of the active sites [26-29]. In this research, we introduce a zeolite A/$ZnCl_2$ nanoparticles as new catalyst used to synthesis pyrazole-1-carbothioamides, candidate for covid-19 main protease (M^{pro}) inhibitor.

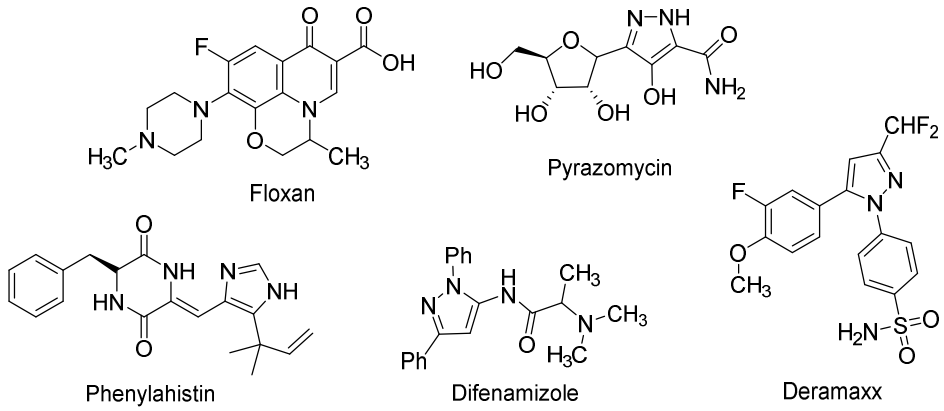

Figure 1. Structures of some bioactive pyrazoles.

RESULTS AND DISCUSSION

XRD experimental data

The XRD pattern of the studied zeolite sample is shown in (Figure 2). Obtained spectra show the crystalline nature of the sample with comparable diffraction to published data of zeolite A (JCPDS 38-0237) revealing intense bands at Braggs angles 2θ = 6.1, 10.0, 12.5, 15.4, 18.5, 21.5, 23.3, 27.6, 29.8, and 34.1° assigned to their corresponding Miller indices (*h k l*) reflection planes (200), (220), (222), (420), (440), (622), (642), (694), and (664) planes of the cubic crystalline system previously indexed by Yao *et al.* [30]. The zeolite A showed the same previously assigned pattern indicating that the structure of the studied material is well retained even after the mailing process.

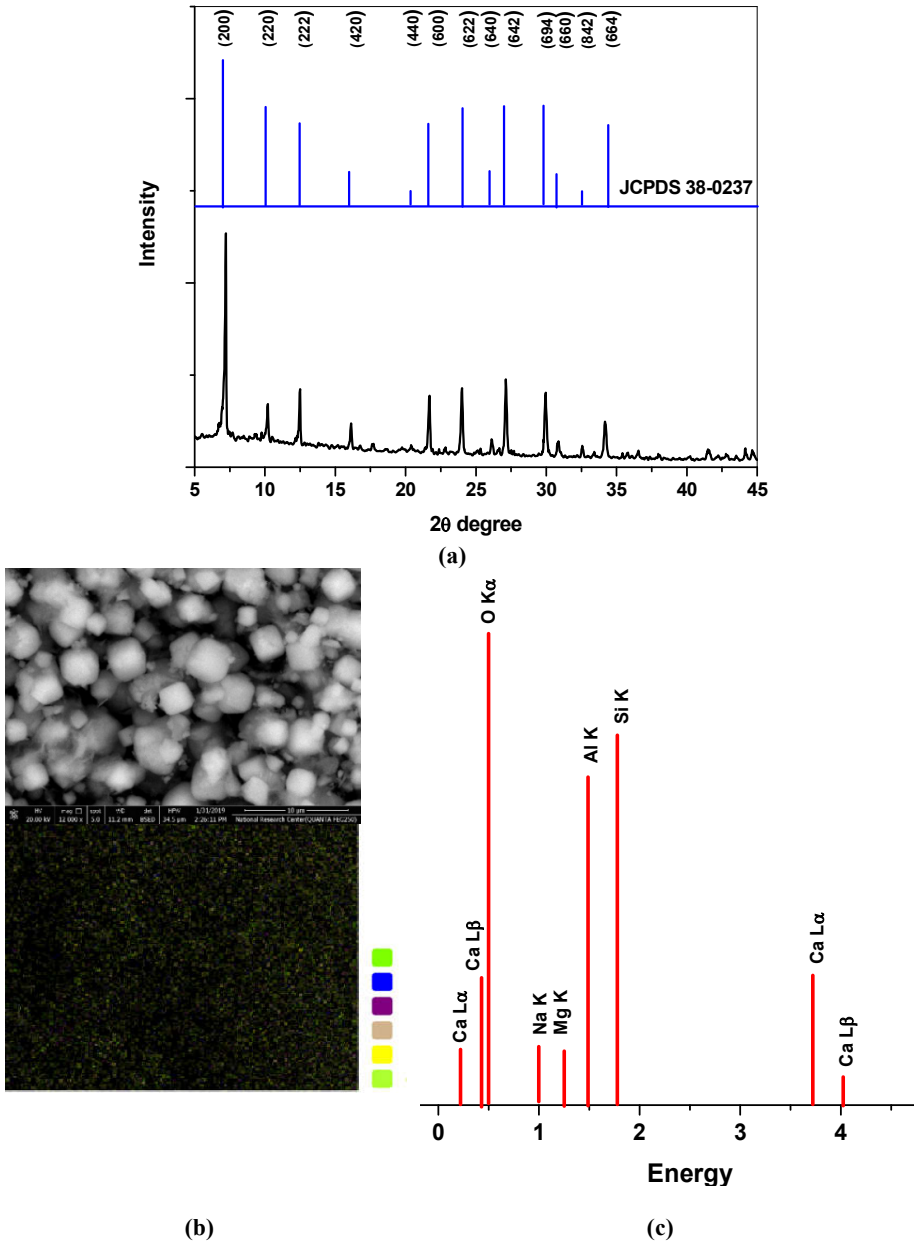

Figure 2. (a) XRD patterns of the studied zeolite A. (b) Magnified SEM image of zeolite A in combination with their mapping. (c) Their energy dispersive X-ray (EDS).

SEM/EDAX/MAP analysis of studied catalyst

Figures (2b and 2c) reveal (b) magnified SEM images of the studied mailed zeolite A sample in combination with their mapping, and (c) their energy dispersive X-ray (EDS).

Captured image mapping shows a homogenous distribution of all constituting elements (Na, Mg, Al, Si, Ca, and O atoms) present inside the chemical structure listed in (Table 1), as well as their atomic and weight percentages. The data also approved that silica is the main constituent along the studied network structure combined with alumina, lime, magnesium, and sodium via oxygen linkages. It was noticed also that the weight fractions of both analyzed silica and alumina are nearly equal.

Table 1. EDS analysis of the studied sample.

Oxide	SiO_2	Al_2O_3	CaO	Na_2O	MgO	Others
Weight%	39.2	38.1	15.5	4.52	2.11	0.57

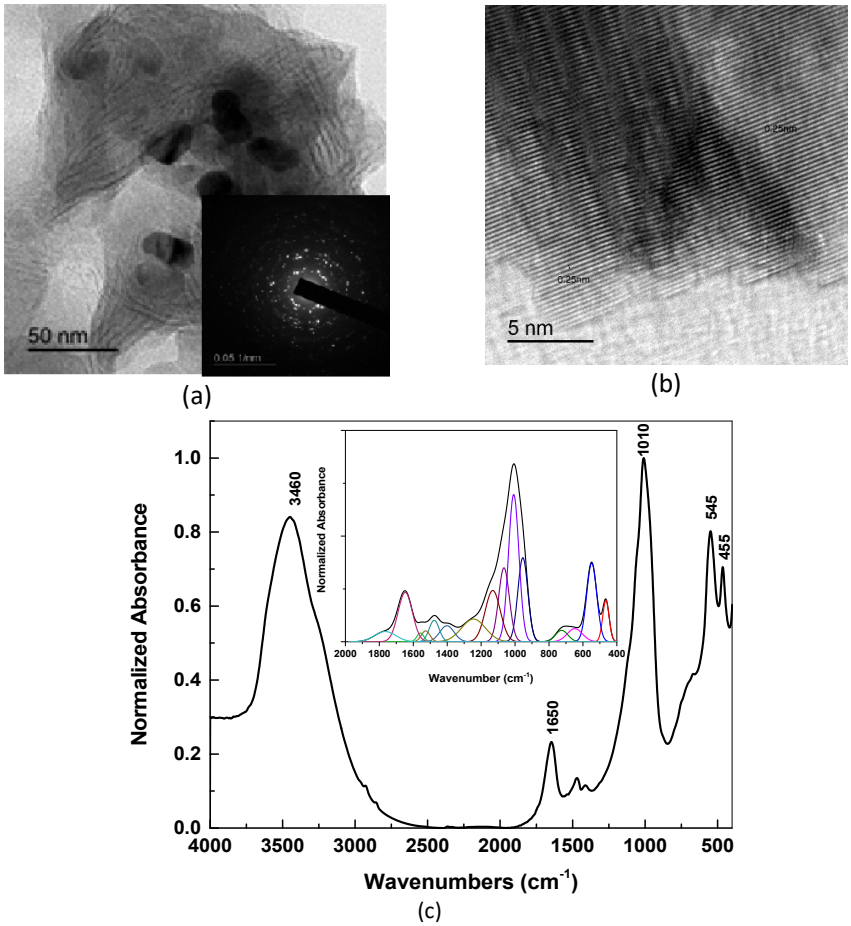

Figure 3. (3a and 3b) HRTEM/SAED images. (3c) FT-IR normalized absorption spectrum of zeolite A.

High-resolution transmission electron microscopy/selected area electron diffraction (HRTEM/SAED)

(Figures 3a and 3b) show high-resolution transmission electron microscope images combined with their selected area electron diffraction (HRTEM/SAED). Studied samples show nearly homogenous morphology with a size ranging between 20-30 nm. In addition, the selected area diffraction pattern (SAED) of prepared nanocrystals reveals a collective pattern of concentric rings with bright spots around a circular path, pointing to a crystalline structure coherent with XRD data.

Fourier transform infrared (FTIR)

(Figure 3c) reveals FTIR optical absorption spectral data of the studied zeolite A sample. Obtained data reveals the following spectral features in correlation with their vibrational groups within the spectral range extending from 4000-400 cm^{-1}. The bands centered at about 3460, and 1665 cm^{-1} attributed to the presence of OH groups resulting from moisture attack when mixing the sample with hygroscopic potassium bromide powder during measurements. Broad, strong band at 1010 cm^{-1} is typically attributed to asymmetric stretching vibrations of silicon and aluminium atoms connected to oxygen atoms inside the network structure [31]. Deconvolution analysis within the spectral range extending between 2000 and 400 cm^{-1} shown in (Figure 5) reveals overlapping peaks attributed to such vibrations. The bands at 554 and 455 cm^{-1} were assigned to external vibrations of double four-rings, and Si-O or Al-O bending vibrations, respectively.

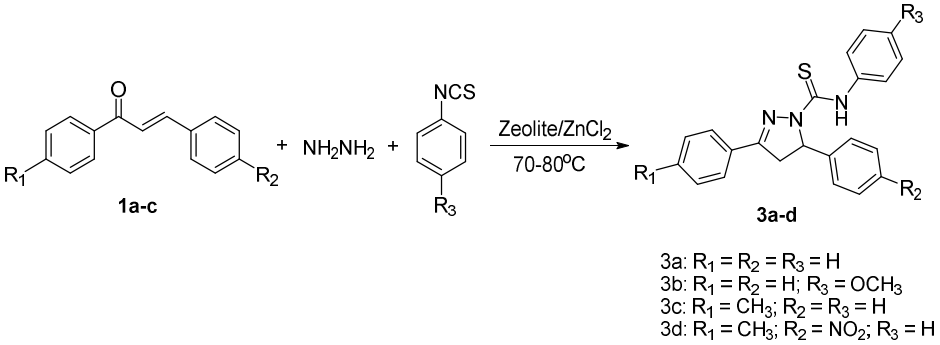

Scheme 1. Synthesis of pyrazole-1-carbothioamides **3a-d**.

Catalyzed synthesis of pyrazole-1-carbothioamides 3a-d

Utilizing catalysis in organic reactions is an endlessly fascinating and ever-changing phenomenon. My research team is continuously looking for new catalysts to characterise and use in the advancement of organic synthesis [32-35]. In this paper, we present a new type of catalyst that can be used to synthesis pyrazole-1-carbothioamides, an important class of organic compounds. We must begin with the optimization step, as is common in this type of reaction for the best reaction condition choice. The reactants (hydrazine hydrate, phenyl isothiocyanate, and unsubstituted chalcone) were mixed as a reference step in the presence of zeolite alone and zinc chloride alone, as well as in the absence of a catalyst. The product was not detected in any of the three cases. That made it obvious that the catalyst, which was present in the form of a zeolite-$ZnCl_2$ mixture, was essential. We started the reaction procedure by mixing the catalyst with hydrazine hydrate, phenyl isothiocyanate for 30 min. Then, the addition of chalcone to the separated product yielded the open structure 2-(3-oxo-1,3-diphenylpropyl)-*N*-phenylhydrazine-1-

carbothioamide (m.p. = 140 °C).When the reaction was repeated with polar solvents like H_2O or ethanol, mixed products-cyclic pyrazole and open structure-was formed. Under solvent-free conditions, the best reaction conditions was initiated by adding 1 mole of chalcone to 1.2 moles of hydrazine hydrate (98%) and 1 mole of phenyl isothiocyanate in the presence of 10 mg of zinc chloride@Zeolite catalyst (Scheme 1). Table 2 shows the application of the reaction on different chalcones and phenyl isothiocyanates.

Table 2. Reaction with different substituted chalcones and phenyl isothiocyanates.

Compound	R_1	R_2	R_3	Molecular formula	Time (h)	Catalyst	Melting point	Yield
3a	H	H	H	$C_{22}H_{19}N_3S$	9	Zeolite/$ZnCl_2$	190 °C	72%
3b	H	H	OCH_3	$C_{23}H_{21}N_3OS$	16	Zeolite/$ZnCl_2$	161 °C	75%
3c	CH_3	H	H	$C_{23}H_{21}N_3S$	11	Zeolite/$ZnCl_2$	165 °C	71%
3d	CH_3	NO_2	H	$C_{23}H_{20}N_4O_2S$	22	Zeolite/$ZnCl_2$	182 °C	78%

Computational studies

The geometries of the pyrazole-1-carbothioamides **3a-d** were optimised using density functional theory (DFT) at the B3LYP/6-311 ++ G (d, p) level [36-38] and implemented in the programme Gaussian 09 W [39]. Frequency calculations show that the optimised geometries are stable, with positive values for all obtained frequencies. Figure 4 depicts the optimised structures, while Figure 5 depicts the patterns of distribution of frontier molecular orbitals; the highest occupied molecular orbitals (HOMOs); and the lowest unoccupied molecular orbitals (LUMOs). In **3a-d** most of the HOMO is localized mainly on thioamide moiety and the pyrazole ring nitrogen atoms with a slight contribution of the phenyl ring-connected to the thioamide. The **3a-c** LUMO has consisted of the π*-orbitals of the 1-thioamide-3-phenyl pyrazole substituents and nitrogens of pyrazole. In **3d**, although the HOMO is similar to other derivatives, its LUMO showed a completely different composition, where it is localized only on the 5-phenyl pyrazole substituent. The HOMO and LUMO energies (E_{HOMO}, E_{LUMO}), besides the HOMO-LUMO energy gap (E_{gap}) are shown in (Table 3). The trend of E_{HOMO} is 3d > 3a≈3c > 3b. The tendency towards decreasing E_{LUMO} is 3d > 3a > 3b = 3c and for E_{gap} 3c = 3a > 3b > 3d. The HOMO energy values for **3a-d** are quite similar, between 5.33-5.67 eV. Also, E_{LUMO} values for compounds **3a-c** are similar between 1.73-1.82 eV. While E_{LUMO} of compound **3d** has a considerably lower value of -3.22 eV, which consequently decreased E_{gap} to 2.45 eV. This may be attributed to 5-phenyl pyrazole's electron-withdrawing NO_2 group.

Table 3. The HOMO Energy (E_{HOMO}), LUMO Energy (E_{LUMO}), HOMO-LUMO Energy Gap (E_{gap}) in eV, electronegativity (χ), global hardness (η), softness (δ) and electrophilicity (ω) values at B3LYP/6-31G* Level of Theory.

Molecules	E_{HOMO}	E_{LUMO}	E_{gap}	χ	η	δ	ω
3a	-5.44	-1.82	3.62	3.63	1.81	0.55	3.65
3b	-5.33	-1.74	3.59	3.54	1.79	0.56	3.49
3c	-5.40	-1.73	3.67	3.56	1.83	0.55	3.47
3d	-5.67	-3.22	2.45	4.44	1.22	0.82	8.06

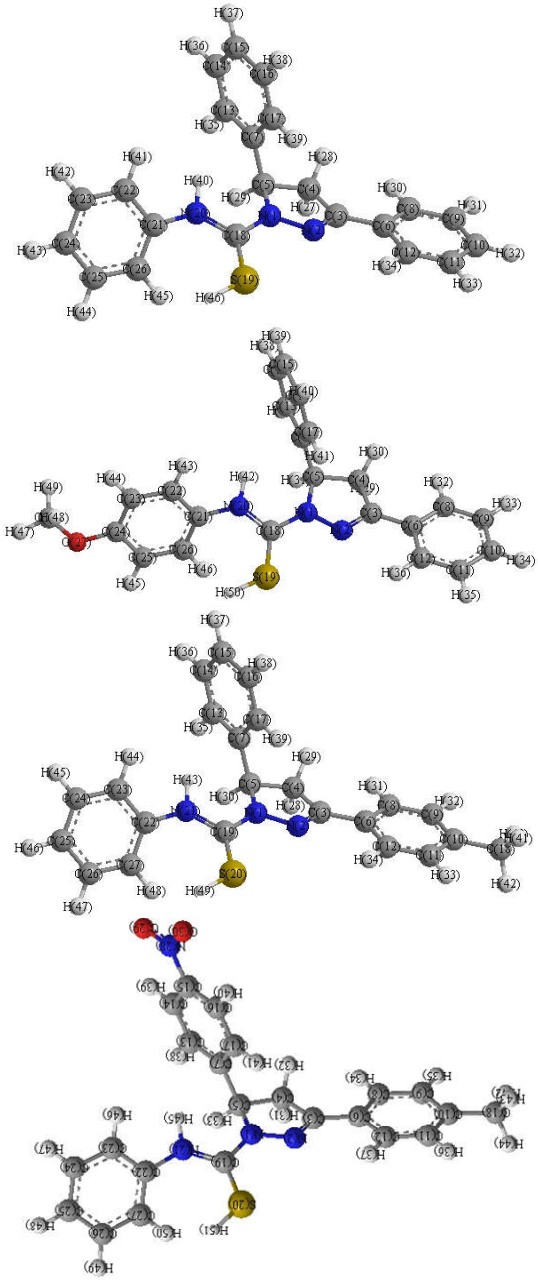

3a

3b

3c

3d

Figure 4. The theoretical optimized structures of the compounds 3a-d with B3LYP/6- 311 ++ G (d, p) method.

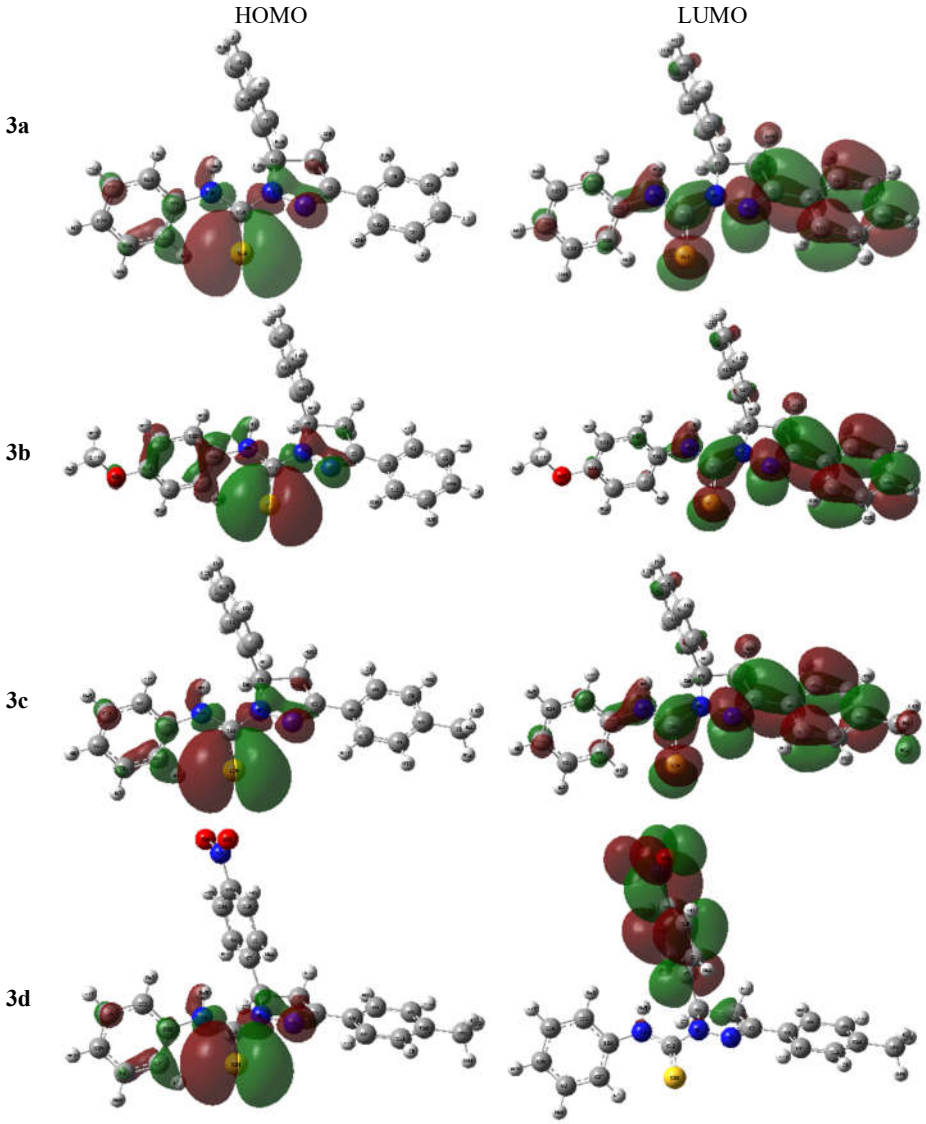

Figure 5. HOMO and LUMO distribution of **3a-d**.

Finally, the calculations of E_{HOMO} and E_{LUMO} enables the calculation of other chemical reactivity descriptors using the following equations [40]:

$$\chi = -\frac{1}{2}(E_{HOMO} + E_{LUMO}) \qquad \eta = -\frac{1}{2}(E_{HOMO} + E_{LUMO})$$

$$\delta = \frac{1}{\eta} \qquad \omega = \frac{\chi^2}{2\eta}$$

Electronegativity (χ), which indicates the acidic or basic character, global hardness (η) which measures the resistance in charge transfer, and global softness (δ) which describes the molecule's ability to receive electrons. Additionally, energy reduction due to HOMO-LUMO electron flow can be measured by electrophilicity (ω). Table 1 shows that the **3d** compound had the lowest global hardness, which was 1.22 eV. On the other hand, the softness is shown in the opposite order, with **3d** being the softest at 0.82 eV.

Molecular docking study

During the past three years, the Corona pandemic has terrified the world. It was necessary to search for an urgent drug to reduce the effects of this epidemic on humans. This is why my research group, [41-45], has made great efforts to search for a cure for this disease. Initially, a theoretical study should be conducted using drug design programs (MOE) on the suitability of the prepared compounds with the protease enzyme. The inhibition of protease enzyme is one of the most important challenges in proposed treatments for Covid-19. The prepared compounds were compared with hydroxychloroquine as a reference compound, and from the theoretical results obtained, it became clear that the prepared compounds gave promising results with the protease enzyme compared to the reference one. The protease active site characterized as Arg 188, Ala 191, Asn 142, Thr 45, Thr 26, Cys 145, Gln 189, Glu 166, His 41, Thr 25, Gln 192, Thr 190, Thr 42, Met 165, Leu 167, Leu 27, Ser 46, Leu 141, Asp 187, His 164, Gly 143, Ser 144, Pro 168, Met 49, Cys 44. (Figure 6) showed the 2D and 3D interaction diagrams of M^{pro}.

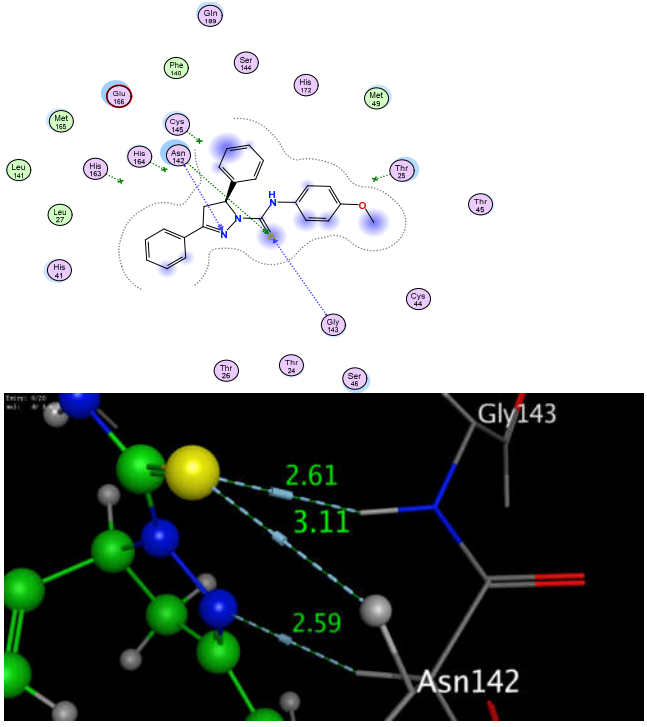

Figure 6. Top: 2D of the (**3b**-M^{pro} active side). Bottom: 3D distance measurements of (**3b**-M^{pro} active side).

The measuring distance between the drug-ligand

There are two electrostatic bonds between the sulfur atom and the amino acid residues Gly143 and Asn142 with distances of 2.61 and 3.11 Å, respectively also there is another bond between the nitrogen atom in the pyrazole ring and Asn142 with a 2.59 Å distance. This compound exhibited 7 intramolecular forces, indicating a high drug-ligand interaction.

EXPERIMENTAL

General remarks

Melting points were determined with Gallenkamp melting point apparatus and are uncorrected. The infrared (IR) spectra were recorded on Thermo Scientific Nicolet iS10 FTIR. ^{1}H NMR and ^{13}C NMR spectra were recorded DMSO-d_6 as a solvent using JEOL's spectrometer at 500 MHz using tetramethylsilane (TMS) as internal standard. Chemical shifts are expressed in δ, ppm. ^{1}H NMR data are reported in order: multiplicity (br, broad; s, singlet; d, doublet; t, triplet; dd, doublet of doublet; m, multiplet), approximate coupling constant in Hertz, number of protons and type of protons. The purity of the compounds was checked by ^{1}H NMR and thin layer chromatography (TLC) on silica gel plates using a mixture of (dichloromethane/methanol) or (petroleum ether/ethyl acetate) as eluent. UV lamp was used as a visualizing agent. Elemental analyses were recorded on Thermo DSQ II spectrometer at Faculty of Science, Alazhar University.

Catalyst preparation

Zeolite A powder combined with $ZnCl_2$ catalyst was synthesized using the hydrothermal method. $ZnCl_2$ (1.36 g) aqueous solution was added to 4.0 g zeolite suspension in a 100 mL Teflon-lined autoclave. The sealed autoclave was then placed in a regulated furnace adjusted at 100 °C for 6 h. The furnace is turned off and left to be cooled at a rate of about 10 °C/h. The dried powder was then kept in a desiccator until use.

General procedure for the synthesis of N,3,5-triaryl-4,5-dihydro-1H-pyrazole-1-carbothioamides ***3a-d***

The reaction was started by mixing chalcone (**1a-c**, 10 mmol) and hydrazine hydrate 80% (1 mL, 20 mmol), the zeolite/$ZnCl_2$ (0.2 g, 20 mol%) was added and the mixture was allowed to stir at 70-80 °C, The reaction was monitored by TLC until 3,5-diphenyl-4,5-dihydro-1*H*-pyrazoles **2a-c** were formed. Then, phenyl isothiocyanate derivative (10 mmol) was added and continued stirring until the reaction completion and this was demonstrated by using TLC. The product was extracted with ethyl acetate (20 mL). Then, the mixture was filtered off and the extract was vaporized. The remaining residue was recrystallized using ethanol to give a pure product.

N,3,5-Triphenyl-4,5-dihydro-1H-pyrazole-1-carbothioamide ***3a***. White powder; yield (72%); m.p. = 188-190°C. IR (ν/cm^{-1}): 3336 (N-H); 2918 (C–H), 1594 (C=N), 1526 (C=C, aromatic). ^{1}H NMR (δ, ppm): 3.13-3.21 (dd, J_1 = 12.00, J_2 = 6.50 Hz, 1H, pyrazole-H), 3.92-3.99 (m, 1H, pyrazole-H), 6.02 (s, 1H, pyrazole-H), 7.14-7.23 (m, 4H, Ar-H), 7.32-7.27 (m, 5H, Ar-H), 7.43-7.56 (m, 6H, Ar-H), 10.19 (s, 1H, NH). ^{13}C NMR (δ, ppm): 42.07, 63.35, 124.89, 125.40 (4C), 127.01, 127.44, 128.01 (3C), 128.61 (2C), 128.69 (2C), 130.78 (2C), 139.50, 142.72, 155.41, 173.71. Analysis calcd. for $C_{22}H_{19}N_3S$ (357.13): C, 73.92; H, 5.36; N, 11.75%; found: 73.81; H, 5.31; N, 11.70%.

N-(p-Anisyl)-3,5-diphenyl-4,5-dihydro-1H-pyrazole-1-carbothioamide ***3b***. White solid, yield = 75%, m.p. = 160-161 °C. IR (ν/cm^{-1}): 3321 (N-H), 2930 (C–H), 1592 (C=N), 1522 (C=C, aromatic). ^{1}H NMR (δ, ppm): 3.21-3.25 (dd, J_1 = 17.50, J_2 = 3.50 Hz, 1H, pyrazole-H), 3.80 (s, 3H, OCH_3), 3.82-3.86 (m, 1H, pyrazole-H), 6.19-6.16 (dd, J_1 = 12.00, J_2 = 3.00 Hz, 1H, pyrazole-H), 6.89 (d, J = 9.00 Hz, 2H, Ar-H), 7.27 (d, J = 7.50 Hz, 2H, Ar-H), 7.27 (s, 2H, Ar-H), 7.46-7.43 (m, 6H, Ar-H), 7.77 (d, J = 8.00 Hz, 2H, Ar-H), 9.11(s, 1H, NH). ^{13}C NMR (δ, ppm): 42.57, 55.37, 63.33, 113.79 (2C), 125.44 (2C), 126.76 (2C), 126.85 (2C), 127.49, 128.84 (3C), 130.91, 131.50, 142.00, 154.92, 157.46, 174.86. Analysis calcd. for $C_{23}H_{21}N_3OS$ (387.14): C, 71.29; H, 5.46; N, 10.84%; found: 71.20; H, 5.42; N, 10.77%.

N,3-Diphenyl-5-(p-tolyl)-4,5-dihydro-1H-pyrazole-1-carbothioamide ***3c***. Pale orange solid, yield = 71%, m.p. = 165-165°C. IR (ν/cm^{-1}): 3297 (N-H), 2921(C–H), 1595 (C=N), 1532 (C=C, aromatic). ^{1}H NMR (δ, ppm): 2.31 (s, 3H, CH_3), 3.22-3.42 (dd, J_1 = 12.50, J_2 = 4.50 Hz, 1H, pyrazole-H), 3.83-3.89 (m, 1H, pyrazole-H), 6.14-6.17 (dd, J_1 = 11.50, J_2 = 3.00 Hz, 1H, pyrazole-H), 7.13-7.19 (m, 5H, Ar-H), 7.35 (t, J = 8.00 Hz, 2H, Ar-H), 7.43-7.47 (m, 3H, Ar-H), 7.65 (d, J = 8.00 Hz, 2H, Ar-H), 7.78-7.76 (dd, J_1 = 4.00, J_2 = 1.50 Hz, 2H, Ar-H), 9.28 (s, 1H, NH). ^{13}C NMR (δ, ppm): 21.10, 42.62, 63.02, 124.17 (2C), 125.34 (2C), 126.85 (2C), 128.52 (2C), 128.83 (2C), 129.49 (2C), 130.68, 130.92, 137.13, 138.99, 155.06, 173.84. Analysis calcd. for $C_{23}H_{21}N_3S$ (371.15): C, 74.36; H, 5.70; N, 11.31%; found: C, 74.21; H, 5.65; N, 11.21%.

5-(4-Nitrophenyl)-N-phenyl-3-(p-tolyl)-4,5-dihydro-1H-pyrazole-1-carbothioamide ***3d***. Yellow solid, yield = 78%, m.p. = 180-182 °C. IR (ν/cm^{-1}): 3296 (N-H), 2919 (C–H), 1595 (C=N), 1532 (C=C, aromatic). ^{1}H NMR (δ, ppm): 2.31 (s, 3H, CH_3), 3.24-3.25 (dd, J_1 = 12.00, J_2 = 4.00 Hz, 1H, pyrazole-H), 3.83-3.89 (m, 1H, pyrazole-H), 6.14-6.17 (dd, J_1 = 11.50, J_2 = 3.00 Hz, 1H, pyrazole-H), 7.13-7.19 (m, 5H, Ar-H), 7.37-7.34 (t, J = 7.50 Hz, 2H, Ar-H), 7.43-7.49 (m, 3H, Ar-H), 7.65 (d, J = 8.00 Hz, 2H, Ar-H), 7.77 (d, J = 8.00 Hz, 2H, Ar-H), 9.28 (s, 1H, NH). ^{13}C NMR (δ, ppm): 21.08, 42.59, 62.99, 124.14 (2C), 125.30, 125.35 (2C), 126.83 (2C), 128.49 (2C), 128.80 (2C), 129.47 (2C), 130.65, 130.89, 137.10, 138.60, 138.97, 155.05, 173.80. Analysis calcd. for $C_{23}H_{20}N_4O_2S$ (416.13): C, 66.33; H, 4.84; N, 13.45%; found: C, 66.49; H, 4.88; N, 13.54%.

CONCLUSION

Zinc chloride@Zeolite catalyst was successfully synthesized via ordinary hydrothermal technique. XRD approves the crystalline nature of synthesized nanoparticles while both SEM/EDAX and HRTEM/SAED show the homogenous morphology with a size ranging between 20-30 nm. The dihydro pyrazole-1-carbothioamide derivatives were successfully synthesized by an eco-friendly method using synthesized and characterized nano Zinc chloride@Zeolite catalyst under solvent-free conditions. The 3D conformation, electronic and charge transfer properties of the synthesized derivatives was investigated by, the density functional theory (DFT) where, the derivative 30d showed the lowest HOMO–LUMO energy gap. Using drug design software, the synthesized pyrazoles can be considered COVID-19 main protease (Mpro) inhibitors.

REFERENCES

1. Kumar, V.; Kaur, K.; Gupta, G.K.; Sharma, A.K. Pyrazole containing natural products: Synthetic preview and biological significance. *Eur. J. Med. Chem.* **2013**, 69, 735-753.
2. Santos, N.E.; Carreira, A.R.; Silva, V.L.; Braga, S.S. Natural and biomimetic antitumor pyrazoles, a perspective. *Molecules* **2020**, 25, 1364.

3. Borthwick, A.D. 2,5-Diketopiperazines: Synthesis, reactions, medicinal chemistry, and bioactive natural products. *Chem. Rev.* **2012**, 112, 3641-3716.
4. Chermahini, A.N.; Teimouri, A.; Beni, A.S.; Dordahan, F. Theoretical studies on the effect of substituent in the proton transfer reaction of 4-substituted pyrazoles. *Comput. Theor. Chem.* **2013**, 1008, 67-73.
5. Catalán, J.; Sánchez-Cabezudo, M.; De Paz, J.L.G.; Elguero, J.; Taft, R.W.; Anvia, F. The tautomerism of 1,2,3-triazole, 3(5)-methylpyrazole and their cations. *J. Comput. Chem.* **1989**, 10, 426-433.
6. Catalan, J.; Elguero, J. *Basicity and Acidity of Azoles* in *Advances in Heterocyclic Chemistry*, Academic Press: New York; **1987**, pp. 187-274.
7. Castaneda, J.P.; Denisov, G.S.; Kucherov, S.Y.; Schreiber, V.M.; Shurukhina, A.V. Infrared and ab initio studies of hydrogen bonding and proton transfer in the complexes formed by pyrazoles. *J. Mol. Struct.* **2003**, 660, 25-40.
8. Hall, D.G. (Ed.) *Boronic Acids: Preparation, Applications in Organic Synthesis and Medicine*, John Wiley and Sons: New York; **2006**.
9. McLaughlin, M.; Marcantonio, K.; Chen, C.Y.; Davies, I.W. A simple, modular method for the synthesis of 3,4,5-trisubstituted pyrazoles. *J. Org. Chem.* **2008**, 73, 4309-4312.
10. Bekhit, A.A.; Hassan, A.M.; Abd El Razik, H.A.; El-Miligy, M.M.; El-Agroudy, E.J.; Bekhit, A.E.D.A. New heterocyclic hybrids of pyrazole and its bioisosteres: Design, synthesis and biological evaluation as dual acting antimalarial-antileishmanial agents. *Eur. J. Med. Chem.* **2015**, 94, 30-44.
11. Sony, J.; Ganguly, S. A battle against aids: new pyrazole key to an older lock-reverse transcriptase. *Int. J. Pham. Pharm. Sci*. **2016**, 8, 75-79.
12. Pai, G.; Chattopadhyay, A.P. N-Arylation of nitrogen containing heterocycles with aryl halides using copper nanoparticle catalytic system. *Tetrahedron Lett*. **2016**, 57, 3140-3145.
13. Alam, R.; Wahi, D.; Singh, R.; Sinha, D.; Tandon, V.; Grover, A. Design, synthesis, cytotoxicity, HuTopoIIα inhibitory activity and molecular docking studies of pyrazole derivatives as potential anticancer agents. *Bioorg. Chem.* **2016**, 69, 77-90.
14. Khanam, H.; Dar, A.M.; Siddiqui, N.; Rehman, S. Synthesis, characterization and anticancer studies of new steroidal oxadiazole, pyrrole and pyrazole derivatives. *J. Saudi Chem. Soc.* **2016**, 20, 7-12.
15. Ardiansah, B.A.Y.U. Recent reports on pyrazole-based bioactive compounds as candidate for anticancer agents. *Asian J. Pharm. Clin. Res*. **2017**, 12, 45-51.
16. Abdel-Wahab, B.F. Pyrazole-3(4)-carbaldehyde: Synthesis, reactions and biological activity. *Arkivoc* **2011**, 1, 196-245.
17. Ilango, K.; Valentina, P. *Textbook of Medicinal Chemistry*, 1st ed.; Keerthi Publishers: India; **2007**; p 327.
18. Song, W.; Haw, J.F.; Nicholas, J.B.; Heneghan, C.S. Methylbenzenes are the Organic reaction centers for methanol-to-olefin catalysis on HSAPO-34. *J. Am. Chem. Soc.* **2000**, 122, 10726-10727.
19. Holderich, W.F.; Bekkum, H. *Introduction to Zeolite Science and Practice.* Bekkum, H. (Eds.), *Studies in Surface Science and Catalysis*; 58; Elsevier: Amsterdam; 1991; p 631.
20. Singh, D.; Prafull, P.; Anuradda, G.; Mahajani, S. Esterification of oleic acid with glycerol in the presence of supported zinc oxide as catalyst. *Ind. Eng. Chem. Res*. **2013**, 52, 14776-14786.
21. Singh, D.; Rohidas B.; Anuradda G.; Sanjay M. Synthesis of biodiesel from vegetable oil using supported metal oxide catalysts. *Energy Fuel* **2014**, 28, 2743-2753.
22. Singh, D.; Anuradda, G.; Sanjay, M. Heterogeneous catalysis for biodiesel synthesis and valorization of glycerol. *Clean Technol. Environ. Policy* **2014**, 17, 1103-1110.
23. Kristiani, A.; Sudiyarmanto, S.; Aulia, F.; Nurul, H. L.; Abimanyu, H. *Metal supported on natural zeolite as catalysts for conversion of ethanol to gasoline.* MATEC Web Conf. 101, 2017.

24. Penzien, J.; Muller, T.E.; Lercher, J.A. Hydroamination of 6-aminohex-1-yne over zinc based homogeneous and zeolite catalysts. *Microporus Mesoporous Mater.* **2001**, 48, 285-291.
25. Azargashb, S.; Sarvary, A.; Hassaninejad-Darzi, S.K. Synthesized NaA nanozeolite as a catalyst for the preparation of 3-aminoimidazo[1,2-*a*]pyridines under solvent-free conditions. *Lett. Org. Chem.* **2022**, 19, 711-718.
26. Yang, X.Y.; Chen, L.H.; Li, Y.; Rooke, J.C.; Sanchez, C.; Su, B.L. Hierarchically porous materials: Synthesis strategies and structure design. *Chem. Soc. Rev.* **2017**, 46, 481-558.
27. Mintova, S.; Jaber, M.; Valtchev, V. Nanosized microporous crystals: emerging applications. *Chem. Soc. Rev.* **2015**, 44, 7207-7233.
28. Mintova, S.; Grand, J.; Valtchev, V. Nanosized zeolites: Quo vadis? *C. R. Chim.* **2016**, 19, 183-191.
29. Roth, W.J.; Nachtigall, P.; Morris, R.E.; Cejka, J. Two-dimensional zeolites: Current status and perspectives. *Chem. Rev.* **2014**, 114, 4807-4837.
30. Yao, G.; Lei, J.; Zhang, X.; Sun, Z.; Zheng, S. One-step hydrothermal synthesis of zeolite X powder from natural low-grade diatomite. *Materials* **2018**, 11, 906-918.
31. ElBatal, F.H.; Abdelghany, A.M.; ElBatal, H.A. Characterization by combined optical and FT infrared spectra of 3d-transition metal ions doped-bismuth silicate glasses and effects of gamma irradiation. *Spectrochim. Acta A Mol. Biomol. Spectrosc.* **2014**, 122, 461-468.
32. Abdel-Latif, E.; Khatab, T.K.; Fekri, A.; Khalifa, M.E. Synthesis of new binary thiazole-based heterocycles and their molecular docking study as Covid-19 main protease (M^{pro}) inhibitors. *Russ. J. Gen. Chem.* **2021**, 91, 1767-1773.
33. Abdelghany, A.M.; Soliman, H.A.; Khatab, T.K. Biosynthesized selenium nanoparticles as a new catalyst in the synthesis of quinazoline derivatives in pentacyclic system with docking validation as (TRPV1) inhibitor. *J Organomet. Chem.* **2021**, 944, 121847.
34. Khatab, T.K.; Kandil, E.M.; Elsefy, D.E.; El-Mekabaty, A. A one-pot multicomponent catalytic synthesis of new 1*H*-pyrazole-1-carbothioamide derivatives with molecular docking studies as cox-2 inhibitors. *Biointerface Res. Appl. Chem.* **2021**, 11, 13779-13789.
35. Khatab, T.K.; Abdelghany, A.M.; Soliman, H.A. V_2O_5/SiO_2 as a heterogeneous catalyst in the synthesis of bis(indolyl)methanes under solvent free condition. *Silicon*, **2018**, 10, 703-708.
36. Frisch, M.J.; Trucks, G.W.; Schlegel, H.B.; Scuseria, G.E.; Robb, M.A.; Cheeseman, J.R.; Fox, D.J. *Gaussian 09 Citation*, Gaussian. Inc.: Wallingford CT; **2009**.
37. Becke, A.D. Density-functional thermochemistry. I. The effect of the exchange-only gradient correction. *J. Chem. Phys*. **1992**, 96, 2155-2160.
38. Lee, C.; Yang, W.; Parr, R.G. Development of the Colle-Salvetti correlation-energy formula into a functional of the electron density. *Phys. Rev. B* **1988**, 37, 785-789.
39. Perdew, J.P.; Wang, Y. Pair-distribution function and its coupling-constant average for the spin-polarized electron gas. *Phys. Rev. B* **1992**, 46, 12947-12954.
40. Xavier, S.; Periandy, S.; Ramalingam, S. NBO, conformational, NLO, HOMO–LUMO, NMR and electronic spectral study on 1-phenyl-1-propanol by quantum computational methods. *Spectrochim. Acta A Mol. Biomol. Spectrosc.* **2015**, 137, 306-320.
41. Naglah, A.M.; Askar, A.A.; Hassan, A.S.; Khatab, T.K.; Al-Omar, M.A.; Bhat, M.A. Biological evaluation and molecular docking with in silico physicochemical, pharmacokinetic and toxicity prediction of pyrazolo[1,5-*a*]pyrimidines. *Molecules* **2020**, 25, 1431-1448.
42. Khatab, T.K.; Mubarak, A.Y.; Soliman, H.A. Design and synthesis pairing between xanthene and tetrazole in pentacyclic system using tetrachlorosilane with aurora kinase inhibitor validation. *J. Heterocycl. Chem.* **2017**, 54, 2463-2470.
43. Abdelghany, A.M.; Khatab, T.K.; Hassan, A.S. Copper-based glass-ceramic as an efficient catalyst in the synthesis of pyrazolo[1,5-*a*]pyrimidine under solvent-free condition with docking validation as Covid-19 main protease (M^{pro}) inhibitor. *Bull. Chem. Soc. Ethiop,* **2021**, 35, 185-196.

44. Sroor, F.M.; Khatab, T.K.; Basyouni, W.M.; El-Bayouki, K.A. Synthesis and molecular docking studies of some new thiosemicarbazone derivatives as HCV polymeraseinhibitors. *Synth. Commun.* **2019**, 49, 1444-1456.
45. Khatab, T.K.; Abdelghany, A.M.; Soliman, H.A. V_2O_5 based quadruple nano-perovskite as a new catalyst for the synthesis of bis and tetrakis heterocyclic compounds. *Appl. Organomet. Chem.* **2019**, 33, 4783.